ASTROBIOLOGY
Volume 8, Number 4, 2008

DOI: 10.1089/ast.2007.0158

Special Paper

Experiment LEND of the NASA Lunar Reconnaissance Orbiter for High-Resolution Mapping of Neutron Emission of the Moon

I.G. Mitrofanov,[1] A.B. Sanin,[1] D.V. Golovin,[1] M.L. Litvak,[1] A.A. Konovalov,[1] A.S. Kozyrev,[1] A.V. Malakhov,[1] M.I. Mokrousov,[1] V.I. Tretyakov,[1] V.S. Troshin,[1] V.N. Uvarov,[1] A.B. Varenikov,[1] A.A. Vostrukhin,[1] V.V. Shevchenko,[2] V.N. Shvetsov,[3] A.R. Krylov,[3] G.N. Timoshenko,[3] Y.I. Bobrovnitsky,[4] T.M. Tomilina,[4] A.S. Grebennikov,[4] L.L. Kazakov,[5] R.Z. Sagdeev,[6] G.N. Milikh,[6] A. Bartels,[7] G. Chin,[7] S. Floyd,[7] J. Garvin,[7] J. Keller,[7] T. McClanahan,[7] J. Trombka,[7] W. Boynton,[8] K. Harshman,[8] R. Starr,[9] and L. Evans[10]

Abstract

The scientific objectives of neutron mapping of the Moon are presented as 3 investigation tasks of NASA's Lunar Reconnaissance Orbiter mission. Two tasks focus on mapping hydrogen content over the entire Moon and on testing the presence of water-ice deposits at the bottom of permanently shadowed craters at the lunar poles. The third task corresponds to the determination of neutron contribution to the total radiation dose at an altitude of 50 km above the Moon. We show that the Lunar Exploration Neutron Detector (LEND) will be capable of carrying out all 3 investigations. The design concept of LEND is presented together with results of numerical simulations of the instrument's sensitivity for hydrogen detection. The sensitivity of LEND is shown to be characterized by a hydrogen detection limit of about 100 ppm for a polar reference area with a radius of 5 km. If the presence of ice deposits in polar "cold traps" is confirmed, a unique record of many millions of years of lunar history would be obtained, by which the history of lunar impacts could be discerned from the layers of water ice and dust. Future applications of a LEND-type instrument for Mars orbital observations are also discussed. Key Words: Moon—Neutron radiation—Hydrogen abundance—Polar cold traps. Astrobiology 8, 793–804.

1. Introduction

Except for the Sun itself, there are 3 large bodies in the inner Solar System that emit gamma rays and neutrons from their surface: the Moon, Mars, and Mercury. The surfaces of the major satellites of the outer planets also produce a variety of nuclear emissions (*i.e.*, all radiated particles and photons from nuclei), provided they do not have a thick atmosphere. Nuclear emissions are produced by bombardment of galactic cosmic rays and, episodically, by solar energetic particles. High-energy protons and nuclei collide with nuclei in the soil to a depth of about 1–2 meters (neutron production level) and produce secondary neutrons with energies about 1–20 MeV. Neutrons diffuse in the subsur-

[1]Institute for Space Research of the Russian Academy of Sciences, Moscow, Russia.
[2]Sternberg Astronomical Institute of Moscow State University, Moscow, Russia.
[3]Joint Institute of Nuclear Energy, Dubna, Moscow.
[4]A.A. Blagonravov Institute of Mechanical Engineering, Moscow, Russia.
[5]Institute of Physics of Nuclear Reactors, Dmitrovograd, Russia.
[6]University of Maryland, College Park, Maryland.
[7]NASA Goddard Space Flight Center, Greenbelt, Maryland.
[8]University of Arizona, Tucson, Arizona.
[9]Catholic University, Washington, DC.
[10]Computer Science Corporation, Greenbelt, Maryland.

face and collide with soil nuclei until they escape from the surface, are absorbed due to capture reaction, or decay due to a finite lifetime. Obviously, neutron emission is associated with the first option only. Neutrons lose energy with collisions; the moderation of energy of escaped neutrons is greater for those particles that have a greater number of interactions. The energy spectrum of emitted neutrons has a thermal component (which corresponds to particles that have been thermalized before escaping) and a power-law tail from epithermal energies up to the original energy of particles that escaped before thermalization (Drake *et al.*, 1988).

Neutron emission is accompanied by the emission of gamma rays from nuclei that were excited by neutrons. The spectrum of nuclear lines from the elements Si, O, Ca, Fe, Cl, H, etc. characterize the composition of the soil. In particular, the line at 2.2 MeV characterizes the abundance of hydrogen because it is produced in the capture reaction $H + n \rightarrow D +$ 2.2 MeV. The energy spectrum of leaking neutrons depends on the composition of the soil and mostly on the content of hydrogen, because H nuclei are the best moderators of neutrons. Even a fraction of hydrogen as small as 100 ppm is known to produce a measurable change of neutron albedo from the surface of celestial bodies with thin or no atmosphere (see below).

Since the first pioneering measurements of nuclear emission from the Moon (Vinogradov *et al.*, 1966; Metzger *et al.*, 1973) and Mars (d'Uston *et al.,* 1989), nuclear methods have become increasingly important in planetology. The main reason for this is the unique ability of nuclear physics to measure, *in situ*, the abundance of many different nuclei in the soil of celestial bodies and, thus, determine the elemental composition of the soil, the content of natural radioactive elements, the fraction of cosmogenic nuclides, etc. The nuclear data also characterize the presence of hydrogen (or hydroxyl) or water in the soil. Orbital observations by the neutron spectrometer on Lunar Prospector (Feldman *et al.*, 1998, 2000; Maurice *et al.*, 2004; Lawrence *et al.*, 2006) have shown that the lunar maps of neutron emission provide evidence of high hydrogen content (or water-ice deposits) in the polar regions. The current data from the Gamma-Ray Spectrometer (GRS) suite of NASA's Mars Odyssey mission (Boynton *et al.*, 2002, 2004; Feldman *et al.,* 2002; Mitrofanov *et al.*, 2002, 2003) have successfully demonstrated the research power of nuclear methods for Mars exploration; the data from GRS has completely changed the previously held view of Mars as a cold, dry planet. At present, several projects with nuclear instruments are either in flight (NASA's MESSENGER to Mercury), in orbit (Japan's Selene), or still in development (NASA's LRO for the Moon, Russia's Phobos-Grunt for Phobos, and NASA's MSL for Mars).

This paper is devoted to the Lunar Exploration Neutron Detector (LEND), which is the large orbital neutron telescope designed to map the Moon's neutron albedo. LEND is Russia's contributed instrument for NASA's Lunar Reconnaissance Orbiter (LRO) (Chin *et al.*, 2007), and its investigation team includes scientists from leading research centers for nuclear and planetary science from both Russia and the United States. LEND is the natural next step in this series of investigations and is based on the available heritage of joint work for neutron mapping of Mars on board Odyssey by the GRS/HEND instrumentation (Boynton *et al.*, 2004). The methods and procedures of LEND data-processing and analysis are based on existing procedures that have been developed for analysis of High Energy Neutron Detector (HEND) data and GRS data.

The scientific goals for testing hydrogen on the Moon's surface are presented in Section 2, and in Section 3 goals for the study of the neutron component of the Moon's radiation environment are discussed. The concept of the LEND design is presented in Section 4. The only new element on LEND in comparison with HEND is the collimator for epithermal neutrons. The physics and method of collimation, as well as results of numerical simulations of LEND investigations, are presented in Section 5. Estimated sensitivity for hydrogen detection for potential cold traps at lunar poles is described in Section 6. Finally, in Section 7 the perspectives of the LEND investigation for future exploration of Moon and Mars are discussed.

2. Requirements for the Testing of Hydrogen and Water Ice on the Moon's Surface

Lunar rocks are made up of minerals that, with a few notable exceptions, are also found on Earth. Silicate minerals, composed dominantly of silicon and oxygen, make up over 90% by volume of many lunar rocks. Oxide minerals, composed chiefly of metals and oxygen, are next in abundance after silicates. They are particularly dominant in the lunar mare basalts and make up about 20% by volume of these rocks. Additional minerals are rare and occur only in small amounts.

Apollo and Luna missions returned to Earth many lunar samples from 9 different sites on the visible hemisphere of the Moon. The lunar probe Clementine returned the first global compositional map of the Moon with a high resolution of 100–200 m per pixel. The Lunar Prospector orbiter mapped the Moon's surface composition with gamma-ray and neutron spectrometers (Feldman *et al.*, 1998, 2000; Maurice *et al.*, 2004; Lawrence *et al.*, 2006). The data are available for 3 models for the lunar surface: the Mare Basalt Model (MBM), the Norites Model (NM), and the Highland Anorthosites Model (HM) (see Table 1). For each model, we postulate a ratio of 40% to 60% between rocks and regolith.

In addition to the elements that make up the soil, the lunar regolith contains elements that are implanted by the solar wind. At a distance of 1 AU from the Sun, the solar-wind

Table 1. Major Element Soil Composition Models (in % by Weight)

Model	*O*	*Si*	*Al*	*Ca*	*Mg*	*Fe*	*Ti*	*Na*
Mare Basalt (MBM)	43.6	21.3	6.6	7.8	5.7	13.4	1.5	0.1
Norites (NM)	45.6	22.9	9.0	7.6	6.8	6.6	1.1	0.4
Highland (HM)	45.7	21.1	15.0	11.7	3.1	3.0	0.2	0.2

proton flux is generally around (1–8) $\times 10^8$ protons/cm^{2}sec. The principal element of the solar wind is H, and the second most abundant element is He, followed by C, N, and O. The solar-wind plasma strikes the lunar surface without significant impedance from a lunar atmosphere or significant repulsion by the Moon's weak, local magnetic fields. The ions imbed themselves in soil grains to a depth of a few atomic diameters.

Lunar soils have also been continually mixed by meteoroid impacts to a depth of at least 2–3 m so that most grains have had substantial exposure on the lunar surface to the solar wind. Soils and regolith breccias typically contain H atoms in bulk concentrations of ~50 ppm. Though mare basaltic rocks have very low hydrogen concentrations, lunar soils and regolith breccias are enriched due to hydrogen implantation by solar wind. According to lunar soil sample studies, the hydrogen content ranges over a factor of 600, from as low as ~0.2 ppm for sample 74220 (Apollo 17) to as high as ~120 ppm for sample 15271 (Apollo 15) (see Haskin *et al.*, 1995). Studies of hydrogen content for different grain-size fractions of soil samples have shown that the hydrogen content is higher in finer grain-size fractions of lunar soil; the hydrogen content in the sample 10084 (Apollo 11) ranges from ~5 ppm for the grain-size fraction 500–1000 μm and up to ~133 ppm for the grain-size fraction <20 μm. The same effect was detected for soil sample 15021 (Apollo 15), for which hydrogen values ranged from ~9 ppm to 148 ppm (for the same grain-size fraction) (Haskin *et al.*, 1995).

It has been shown that soils with low H concentrations are "immature," *i.e.*, most of their grains have not been exposed on the lunar surface long enough to approach the saturation level of H. As laboratory studies of the lunar samples have shown, the hydrogen content correlates with the index of maturity; higher content of hydrogen was found in soils with higher index of maturity. In general, the maturity index and, correspondingly, H content increase in the upper layers of regolith, and the highest values are within a few tens of centimeters of the surface.

According to Lunar Prospector data (Feldman *et al.*, 1998, 2000; Maurice *et al.*, 2004; Lawrence *et al.*, 2006), the neutron flux from the Moon has depressions above the northern and southern polar regions. The decrease of epithermal neutrons is about 3% and 5% in the north and south, respectively. The best spatial resolution of these regions, full width at half maximum = 45 km, was obtained during the low-altitude (30 km) orbital stage of the mission.

Radar sounding data from Clementine has identified possible deposits of water ice in deep polar craters (Nozette *et al.*, 1996). As the first explanation of these neutron depression features, Feldman *et al.* (1998) suggested that they are related to water-ice deposits in permanently shadowed regions. The very small (1.5°) inclination angle of the Moon's equator to the ecliptic leads to the speculation that there may be water ice preserved in the permanently shadowed craters of the pole—cold traps. The maximal temperatures in the near-polar craters do not exceed the limit of temperatures for evaporation of water ice or other volatile deposits. This water ice and deposits of volatiles may originate from comets that struck the Moon long ago.

Another model suggests (*e.g.*, Crider and Vondrak, 2000) that the enhancement of hydrogen content in the polar subsurface is due to much lower surface temperatures than is the case at polar latitudes. The content of implanted gases in the lunar regolith is controlled by the desorption rate from the implanted layers of particles. In polar regions, diffusion and desorption are thought to become so slow that the implanted atoms are "frozen" into regolith particles. So the maximal concentration of implanted atoms could be reached in these regions. The lunar exosphere and Earth's magnetosphere supply the solar wind gases into the permanently shadowed craters, where the gases can be trapped and preserved in the regolith. This effect may be responsible for the hydrogen enrichment of the lunar polar regions observed by Lunar Prospector. However, as concluded (Feldman *et al.*, 1998, 2000; Maurice *et al.*, 2004; Lawrence *et al.*, 2006), the data from Lunar Prospector are thought to indicate that the polar regions have an enhanced content of implanted hydrogen in the soil, with at least some fraction of hydrogen in the form of water ice.

Therefore, according to the present knowledge of the surface distribution of hydrogen on the Moon, there are 2 general questions the LEND investigation will attempt to answer:

Task 1: Determine the origin of "neutron depressions" in the polar regions of the Moon. The question is whether they are due to enhancement of implanted hydrogen from solar wind as a result of the much colder surface of the polar regions or if deposits of water ice from comet impacts accumulated in polar cold traps. To accomplish this task, LEND will map epithermal neutrons at the polar regions with a spatial resolution of about 5 km and a sensitivity for detection of hydrogen at the level of 100 ppm (see Table 2). This data, when combined with data from other instruments on LRO—surface relief data from the Lunar Orbiter Laser Altimeter (LOLA), surface temperature data from the Diviner Lunar Radiometer Experiment (DLRE), and data for Lyman-alpha albedo from the Lyman-Alpha Mapping Project (LAMP) will allow a comparison between areas of depressed neutron emission in permanently shadowed regions at the lunar poles. LEND will also provide measurements of the spatial variation of high-energy neutrons from the Moon (see Table 2). Joint analysis of data for epithermal and high-energy neutrons may allow for a distinction between regolith with homogeneous composition and a layered subsurface with either water ice on top of a dry soil or the inverse.

Task 2: Determine the variation in hydrogen content at moderate latitudes of the Moon in comparison to surface variations of minerals, thermal conductivity, and soil maturity. A neutron spectrometer on Lunar Prospector has already provided global mapping data for hydrogen by way of a non-collimated omni-directional detector (Feldman *et al.*, 1998, 2000; Maurice *et al.*, 2004; Lawrence *et al.*, 2006). To solve this task with higher spatial resolution, LEND will provide global maps of epithermal emission and high-energy neutrons with a spatial resolution of 20–30 km (see Table 2). Analysis of these data will allow for an estimate of the spectral density of neutron flux for different provinces of the Moon with different geochemical, geologic, and thermal properties. It will also facilitate a determination of the correspondence or correlation between them.

During the investigation of both Tasks 1 and 2, knowledge of the elemental composition of lunar regolith in the shallow surface must also be taken into account. In general, the leakage flux of neutrons is determined by the efficiency of the neu-

tron moderation process and total cross section for absorption. Though the leakage flux is essentially dependent on the hydrogen content, it depends, in part, on the regolith composition. Several elements in particular may change the leakage flux of thermal and epithermal neutrons in the soil due to strong absorption effects. Generally speaking, the gamma-ray lines of all soil-composing elements and the flux of outgoing neutrons should be measured so as to estimate the content of hydrogen along with the composition of all the other elements. A comprehensive method such as this was employed by the GRS investigation on the NASA Mars Odyssey mission (Boynton *et al.*, 2004). LRO will not perform measurements of gamma-ray emission, but data from the previous US mission Lunar Prospector and the Japanese mission Selene shall be used for joint analysis with LEND neutron data. In particular, the surface distribution of the KREEP group of elements (*i.e.*, K, potassium; REE, rare earth elements; and P, phosphorus), where local enhancements have been detected at moderate latitudes (Metzger *et al.*, 1973), should be taken into account. This group is known to contain Gd and Sm, which are strong absorbers of low energy neutrons. To accomplish Tasks 1 and 2, we will produce hydrogen maps by combining available gamma-ray data with LEND neutron data corrected for the variation in KREEP element concentrations at the surface. Knowledge of surface distribution of KREEP elements would be improved by use of LEND neutron mapping data measured with higher spatial resolution.

Task 1 has significant astrobiological applications: if the presence of water-ice deposits in polar cold traps is confirmed by orbital mapping of neutron emission, astrobiologists will obtain a unique record of many millions of years of lunar history. Indeed, the first layer of water ice was formed at the bottom of shadowed craters by vapor deposited by comet impacts after the impact crater was formed by itself or after the Moon had developed the current conditions for shadowing from sunlight. This could have taken place some hundreds of millions of years ago. Each subsequent meteorite or comet impact would add to the sequence stratigraphy of water ice or dust layers preserved at the lunar poles. There is no other place in the Solar System where the record of Solar System history is so well preserved. Collision rates and masses, as well as the composition of comets and asteroids, could be determined from studies of these layers.

Moreover, some biosignatures could reside in these ice layers, in the event that cometary ice had ever delivered a "seed of life" as ascribed to the panspermia hypothesis. All other places in the Solar System with similar potential for containing biosignatures will not be visited in the foreseeable future by space probes. Therefore, detection of water-ice deposits in the polar cold traps of shadowed craters will be equally important for fundamental science as well as for engineering and creation of the habitable infrastructure of a Moon base.

Table 2. Main Measurements and Data Products from LEND Investigation

LEND sensors	*Performed measurements*	*Correspondence with tasks of LEND investigations*
Collimated ^{3}He counters CSETN 1–4	Measure epithermal neutrons from the Moon around nadir direction with total counting rate 2.1 counts/s and narrow FOV with opening angle 5.6° (HWHM)	Detection of spatial variations of emission of epithermal neutrons shall allow mapping of the content of hydrogen in the shallow subsurface (relevant to Tasks 1 and 2)
Collimated scintillation sensor SHEN	Measure high-energy neutrons 0.3–15 MeV from the Moon around nadir direction with total counting rate 5.5 counts/s and narrow FOV with opening angle 20° (HWHM)	Detection of spatial variations of emission of high-energy neutrons at polar regions of the Moon shall allow testing of the presence of layering deposits of water ice (relevant to Task 1)
Sensors STN1 and SETN	Measure thermal and epithermal neutrons from the lunar surface and produced by LRO material under the action of galactic cosmic rays and solar particle events	Characterization of neutron component of radiation environment above all lunar surface at the altitude of LRO orbit for condition of quiet Sun, for periods of crossing the tail of Earth's magnetosphere, and for periods of solar particle events (relevant to Task 3)
Sensors STN 2 and 3	Measure thermal neutrons from front and back sides of LRO orbital flight to use the Doppler-filter technique for distinction between the local neutron background of LRO and neutron emission from the Moon	

3. Characterization of the Neutron Component in the Radiation Background

As is the case for water and mineral resources, properties of the radiation environment on the surface of the Moon should be well understood before further exploration of this celestial body. The neutron component of this environment is known to be an important factor in terms of the radiation risk for humans. A detailed characterization of neutron energy/angle/flux parameters around the Moon and on the surface is another major activity of the LEND investigation:

Task 3: Determine the spectral density of the neutron flux over a broad energy range from thermal particles up to MeV neutrons both for quiet solar periods, when neutrons are produced by galactic cosmic rays, and for time intervals of solar particle events, when the neutron fluence is known to become much larger than during quiet solar conditions.

To address Task 3, LEND data will be used to compile a global map of the neutron component of the lunar radiation environment over the broad spectral range, from thermal energy up to MeV (see Table 2). For omni-directional orbital neutron detectors, the scale of surface resolution is about 1.5 times the altitude (*e.g.*, see Maurice *et al.*, 2004). So, for an LRO altitude of 50 km, the resolution of LEND's map of the radiation environment will be about 75 km.

4. Conceptual Design of LEND

The Russian-made, Russian-supplied LEND instrument (Figs. 1–3) was developed at the Institute for Space Research by order of the Federal Space Agency of Russia in accordance with an Implementation Agreement between NASA and the Federal Space Agency. The concept of this instrument was determined in accordance with the measurement requirements necessary to accomplish Tasks 1–3 (see Table 2). LEND is the younger brother of another Russian instrument, HEND (High Energy Neutron Detector), which continues to perform well in its eighth year of science measurements on board NASA's Mars Odyssey mission (Mitrofanov *et al.*, 2002; Boynton *et al.*, 2004). LEND and HEND have similar types of neutron sensors, and valuable science data from HEND about martian water resources has demonstrated the suitability of these sensors for purposes of orbital "neutronography" of a planet. The major distinction of LEND from HEND is the presence of a collimation module, which absorbs neutrons from outside a narrow Field of View (FOV).

The concept of neutron collimation is presented in Fig. 1. The neutron collimator provides the instrument FOV: epithermal neutrons of direct flux inside the FOV are recorded by the detector (see emission point A, Fig. 1), while the major fraction of neutrons outside the FOV are absorbed by the collimator. This collimation technique provides mapping of epithermal neutrons from the Moon's surface with the horizontal resolution of 5 km for LRO at an altitude of 50 km (see Section 5).

LEND will be the first neutron telescope for accurate imaging of lunar emission of epithermal neutrons (Fig. 2). The primary type of LEND sensor is ^{3}He counter LND 253141, which is used for 8 LEND sensors: for 4 Collimated Sensors of EpiThermal Neutrons (CSETN 1–4), for 3 Sensors of Thermal Neutrons (STN 1–3), and 1 Sensor of Epithermal Neutrons (SETN) (Fig. 3). The ^{3}He nucleus has one neutron less than the main isotope of Helium (^{4}He, or alpha particle), and it has a large cross section for capture of low-energy neutrons in the reaction n + ^{3}He → ^{3}H + p + 764 keV. The re-

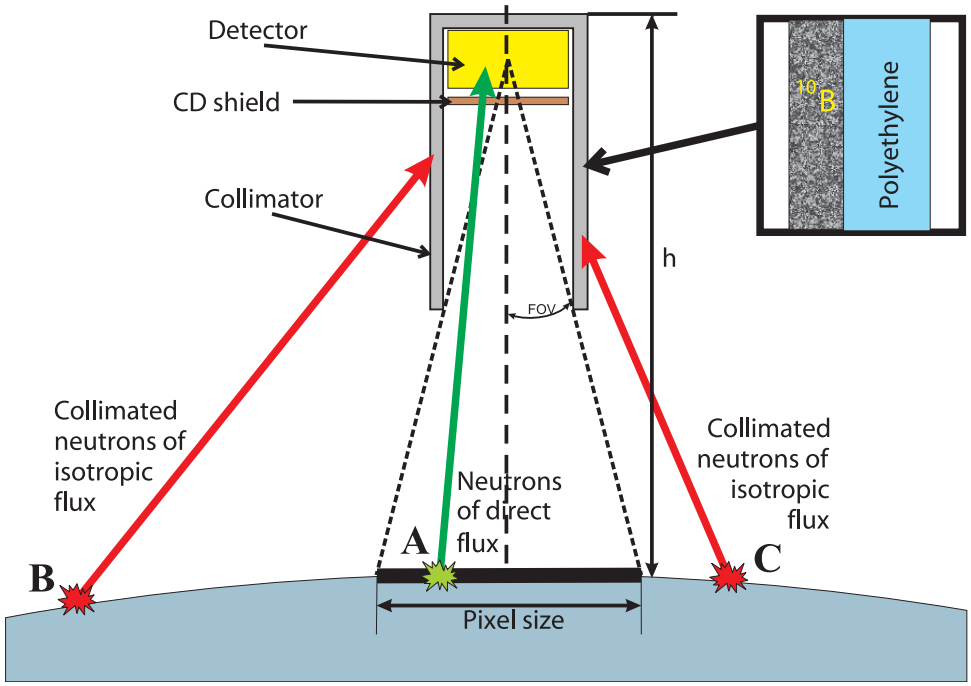

FIG. 1. Schematic concept of neutron collimation: the layer of ^{10}B is inside and the layer of polyethylene is outside the collimator.

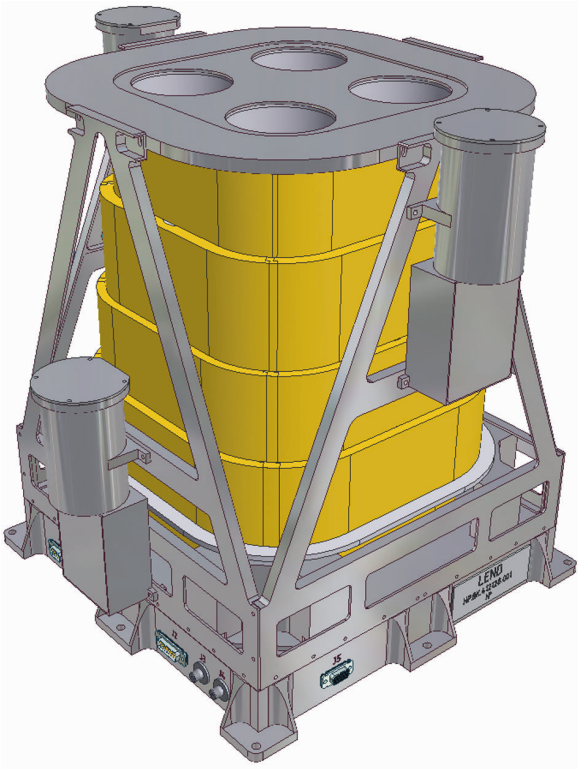

FIG. 2. General view of the LEND engineering unit.

leased energy of the reaction is distributed between a triton ^{3}H and proton with 191 keV and 573 keV energies, respectively, in inverse proportion to their masses, 3:1. The ^{3}He counter produces electrical counts proportional to the rate of neutron detection.

The Collimated Sensors of Epithermal Neutrons, CSETN, are enclosed by Cd shields that absorb all neutrons with energies below ~0.4 eV, which mainly correspond to thermal neutrons. Another sensor with a Cd shield is the external Sensor of EpiThermal Neutrons (SETN) at the top of the instrument (Fig. 3), which detects epithermal neutrons from all directions around the instrument. Three other external Sensors of Thermal Neutrons (STN 1–3) detect thermal and epithermal neutrons. One of them, STN 1, is also at the top of the instrument, and it detects particles from all directions. The combination of 2 external counters, SETN and STN 1, will allow the measurement of local density of thermal and epithermal neutrons around the spacecraft.

Two other external thermal counters, STN 2 and 3, are located near the midpoint of the instrument (Fig. 3). They have the thick mass of the collimation module between them. For sensors on the +X and −X sides, the collimation material absorbs all external particles coming from directions −X and +X, respectively. The velocity vector of LRO will correspond to 1 of these directions; therefore, sensors STN 2 and 3 will detect neutrons with velocities ($V_n + V_{orb}$) and ($V_n - V_{orb}$), respectively, and operate as a Doppler filter to separate the flux of external neutrons from the Moon and the flux of local neutrons from the spacecraft. The concept of the Doppler filter for neutron detectors on the orbit was suggested in Feldman and Drake (1986). The full set of all 4 sensors, SETN and STN 1–3, will provide the data for Task 3: to characterize the neutron component of lunar radiation background at the altitude of LRO separately from the neutron component of local background produced by LRO itself.

Four ^{3}He counters, CSETN 1–4, are installed inside the collimating module, which effectively absorbs external neutrons outside of the instrument FOV (Fig. 3). This method of high spatial resolution "neutronography" of another planet will be performed for the first time by the LEND telescope. Absorbing neutrons effectively is very difficult; one of the best absorbing materials is ^{10}B, and its absorption efficiency becomes much higher when neutrons are slower. For LEND, we will use collimators for each counter CSETN 1–4 with external layers of polyethylene for moderation of impacting neutrons and internal layers of ^{10}B for their efficient absorption (Figs. 1 and 3).

For a neutron instrument with the required H sensitivity in combination with fine spatial resolution, the total mass of the detection-and-collimation segment is primarily determined by the size of the sensors and the FOV. However, there is still a rather large number of additional collimator parameters that must be optimized. This work has been performed during the LEND design, and the results are presented in Section 5. The imaging capability of LEND for emission of epithermal neutrons from the Moon is accomplished with the narrow FOV of 5.6° opening angle (Half Width Half Maximum). This FOV and the sizes of the ^{3}He counters, CSETN 1–4, were determined by the numerical optimization procedure driven by the requirements of Tasks 1 and 2.

A second type of LEND sensor is the Sensor for High Energy Neutrons (SHEN), which is a stilbene scintillator (Fig. 3) that produces a flash of light each time a high-energy neutron in the range 0.3–15.0 MeV collides with a hydrogen nu-

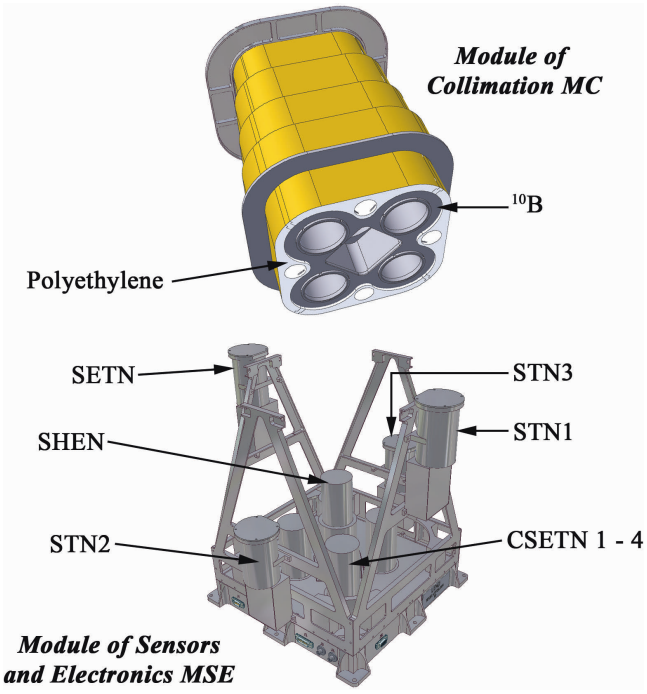

FIG. 3. Two modules MSE and MC with all 9 sensors of LEND and electronics.

cleus and creates a recoil proton. Special shape-sensitive electronics distinguishes proton counts from electron counts, and an active anti-coincidence shield eliminates external charged particles. This sensor is installed inside the central hole of the collimation unit, and its FOV corresponds to 40° Half Width Half Maximum (HWHM).

At this time, LEND development is already at a rather mature stage of manufacturing; therefore, all these parameters are reliably known. LEND includes 2 separable modules: the Module of Sensors and Electronics (MSE) and the Module of Collimation (MC) (Fig. 3). The MC is integrated with the MSE by 4 triangular fixture frames and 4 supporting elements at corners of the MSE main box, and it has no other mechanical contacts with the MSE structure. Therefore, the MC modules may be changed between different MSE modules, which allows for simpler testing and validation and significantly reduces instrument cost.

The mechanical design of the MSE is rather simple (Fig. 3). It has a main box for electronics with the instrument footprint at the bottom and 5 collimated sensors at the top: four CSETN 1–4 at the corners and SHEN in the center. Four external counters, SETN and STN 1–3, are attached to the triangular frames, which also support the MC. These sensors are connected by internal cables with the main electronics box. The mechanical design has been supported by numerical modeling of its mechanical structure to obtain the most efficient usage of limited mass of the instrument, about 26 kg for the highest sensitivity of the instrument. All metallic elements of MSE are made from magnesium to decrease the total instrument mass, and all structural elements were optimized, taking into account the required safety factors and fundamental frequency value (*e.g.*, see Bobrovnitskii, 2001; Tomilina *et al.*, 2003). A positive result of mechanical optimization has been validated by instrument environmental tests for shocks and vibrations.

The thermal design of LEND has also been accompanied by the thermal numerical model at the component scale. The base of MSE is in thermal contact with the spacecraft science deck, and it is covered by a multi-layer insulation blanket.

Electrical subsystems of MSE are the following: eight identical analog boards for ^{3}He counters; CSETN 1–4; SETN and STN 1–3; analog boards of scintillation sensor SHEN; two high-voltage boards; secondary power board; and central logic and digital board. All these boards have the heritage of the HEND design; it could be said that LEND is, electronically and logically, nearly identical to HEND. The logic of LEND operations is based on RTAX series Actel FPGA. It is very simple in that it performs digitalization of counts of all 9 sensors, supports the anti-coincidence system for SHEN, makes a data frame with counts from all 9 sensors of LEND, allows changes of high-voltage level and discrimination levels, accepts commands, and sends telemetry data by a 1553 interface.

The conceptual design of the MC is quite new. It has 4 collimation holes for CSETN 1–4 and one central collimation hole for SHEN. Four collimation holes for CSETN represent the well-known physical concept of absorption of epithermal neutrons: first, to moderate neutrons in polyethylene and, second, to absorb them in ^{10}B. The central collimation hole for the SHEN is formed by the external polyethylene elements of the 4 major collimators for CSETN. The SHEN has a low-energy cutoff at 300 keV, and collimation for this sensor is based on moderation of high-energy neutrons in the polyethylene wall below this threshold.

The configuration of the MC was based on numerical optimization in accordance with the requirements of necessary spatial resolution of the instrument and limited mass available for LEND (Section 5). The physics of neutron detection ultimately dictates the level of sensitivity and spatial resolution for any given mass of a neutron telescope: any improvement in these 2 parameters requires a more massive collimator. The total mass of the LEND MC is about 16 kg. However, there are several other collimator parameters, such as the shape, the thickness of moderating and absorbing layers, and the form of ^{10}B material, all of which provide the best collimation efficiency for an MC of a given mass. The structure of the MC contains 5 enclosed sections; the internal volume of each section contains elements of polyethylene and ^{10}B powder (Fig. 3). The density of the powder is 0.9 g/cm^3, and the weight fraction of the ^{10}B isotope of boron is 0.97. Elements of polyethylene are also fixed outside the enclosure (Fig. 3).

5. Numerical Optimization and Validation of the LEND Collimator

The flux of neutrons from the Moon depends on the elemental composition of the soil and the content of hydrogen in the subsurface. We have performed numerical modeling of the neutron emission from the Moon using the MCNPX code for 3 main models of soil composition (Table 1), with different content of hydrogen or different layering of water-ice deposits, or both. LEND was assumed in the models to be in a polar circular orbit at an altitude of 50 km, and the flux of neutrons was calculated according to numerical simulation of neutron emission of the Moon due to galactic cosmic rays.

For simulation of LEND measurements, it was assumed that the test spot with hydrogen has an angular size θ_{spot} comparable with the opening angle θ_{FOV} of the collimator FOV (Fig. 1). The number N_{signal} of detected neutrons from the test spot is

$$N_{signal} = \pi\, \theta_{spot}^2\, F_{spot}\, \varepsilon\, S_{det}\, t_{exp}, \quad (1)$$

where F_{spot} is a neutron flux from point A of the spot, neutrons $\cdot$ cm^{-2} $\cdot$ ster^{-1} $\cdot$ s^{-1} (Fig. 1), ε is the efficiency of the detector with area S_{det}, and t_{exp} is the total exposure time. The collimator has a small but non-zero transparency. Some number of neutrons, N_{iso}, outside of the test spot (as emission points B and C in Fig. 1) may also be detected. The total number of detected counts is $N_{tot} = N_{signal} + N_{iso}$.

To perform detection of hydrogen in the test spot, one has to measure the variation $\delta \cdot N_{signal}$ of counts from the tested spot in comparison with counts from a similar non-hydrogen spot, and this measured value should have high significance in respect to random fluctuations of counts. For a particular measurement, a standard variation of counts $\sigma = N_{tot}^{1/2}$ is contributed by total counts in the LEND detectors. The requirement of measurements of neutron flux relative variations δ with 3σ significance corresponds to the condition

$$\delta \cdot N_{signal} \geq 3\, (N_{signal} + N_{iso})^{1/2}. \quad (2)$$

A collimator with $\theta_{FOV} \sim \theta_{spot}$ is considered to be well designed for the detection of hydrogen in the test spot if

$N_{signal} > N_{iso}$. However, the condition $N_{signal} >> N_{iso}$ becomes excessive when the collimator becomes too heavy for a realistic spaceflight instrument: in an optimally collimated instrument, $N_{signal} \sim N_{iso}$. For narrow FOV, $\theta_{FOV} \sim 0.1$ radians, this condition is satisfied provided that the transparency of the collimator is about 0.01 or smaller. We have studied different materials that provide such a high shielding efficiency. At present, we have demonstrated that a double-layered structure with an external layer of polyethylene-like material and an internal layer of ^{10}B-rich material provides the necessary shielding.

Counting statistics should provide the required sensitivity for detection of regional variations δ of neutron flux. Established threshold values of δ_{det} are transformed into the corresponding content of detectable hydrogen according to the Monte Carlo numerical model for epithermal neutrons produced by the Moon (Fig. 4). For all 3 composition models, the presence of 100 ppm of hydrogen leads to decrease of emission of epithermal neutrons by about $\delta_{det} = 0.05$.

The present design of LEND was developed by a special program of numerical optimization of collimator shape and layering, in which several free design parameters were varied to obtain the highest sensitivity within a limited collimator mass. This program was based on the Monte Carlo model for the angular and energy distribution at 50 km for neutrons coming from the lunar surface based on a standard highland regolith composition (Table 1). We have performed numerical calculations for LEND collimated neutron detectors with different configurations of layers of polyethylene-like material and ^{10}B-rich material. The differential and integral "collimation curves" produced as a result of these optimization calculations, which are presented in Fig. 5, reveal the distribution of counts in the detector for different impact angles of detected neutrons. The sharp decrease in the differential collimation curve for angles >10° is due to the absorption of neutrons by the walls of the collimator. The integral collimation curve (Fig. 5) demonstrates how the count rate of "signal" increases with the increasing size of the test spot on the surface. According to these numerical simulations, the expected total counting rate of all 4 sensors CSETN 1–4 at an altitude of 50 km is about $C_{tot} = 2.1$ counts/s. Due to collimation, these counts are distributed along the angle θ in accordance with the differential collimation curve (Fig. 5). A test spot with a radius of 5 km will contribute a "signal" of about $C_{signal} = 0.9$ counts/sec; and, correspondingly, all other surfaces will contribute about 1.2 counts/sec of "noise." The signal to noise ratio is about 0.75 in this case.

This value of signal count rate is about 3 times higher than the value for signal $C_{signal}' = 0.32$ counts/sec, which we have estimated numerically for an instrument with a simple cylindrical collimator design. Using the simplest scaling approach, one may deduce practically the same value for the signal count rate $C_{signal}'' = 0.29$ counts/sec, using the measured count rate of $C_{LP} = 21$ counts/sec from the non-collimated neutron detector of Lunar Prospector (Maurice *et al.*, 2004). So, the optimization program for the LEND collimator has allowed us to obtain a signal count rate, $C_{signal} = 0.9$ counts/sec, about 3 times higher than rates predicted by the simplest approaches.

One may estimate the total statistics of N_{signal} and N_{tot}, as the product of counting rates C_{signal} and C_{tot}, respectively, and the exposure time t_{exp}. Thus, Eq. 2 becomes the simple relation

$$\delta_{det}\, C_{signal}\, t_{exp}^{1/2} = 3\, N_{tot}^{1/2} \quad (3)$$

between the total exposure time t_{exp} of a test spot and detectable relative variation δ_{det} of neutron emission (at the significance level of 3σ). Exposure time of a test spot depends on its size and position on the Moon. The formal mission requirement of LRO (Chin *et al.*, 2007) states that LEND will "determine hydrogen content of the subsurface at the polar regions with spatial resolution of 10 km and with sensitivity to concentration variations of 100 parts per million (ppm) at the poles." Exposure time $t_{exp}^{(pole)}$ of a polar test spot with a diameter of 10 km is about 3×10^4 sec. Using 0.9 counts/sec

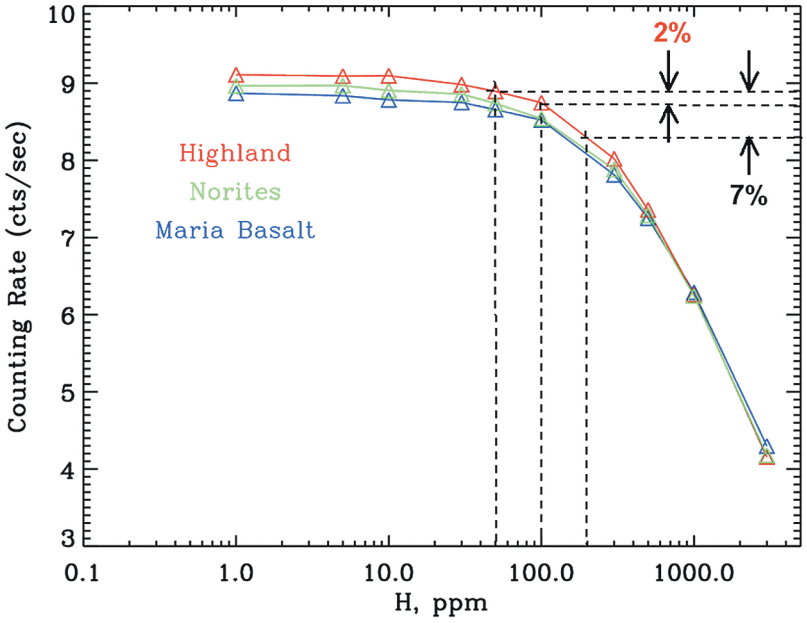

FIG. 4. Decrease of count rate of epithermal neutrons in ^{3}He sensor (diameter 5 cm, pressure 20 atm) at 50 km altitude above the Moon as function of content of hydrogen in the soil (ppm). Three models of lunar soil are shown (Table 1).

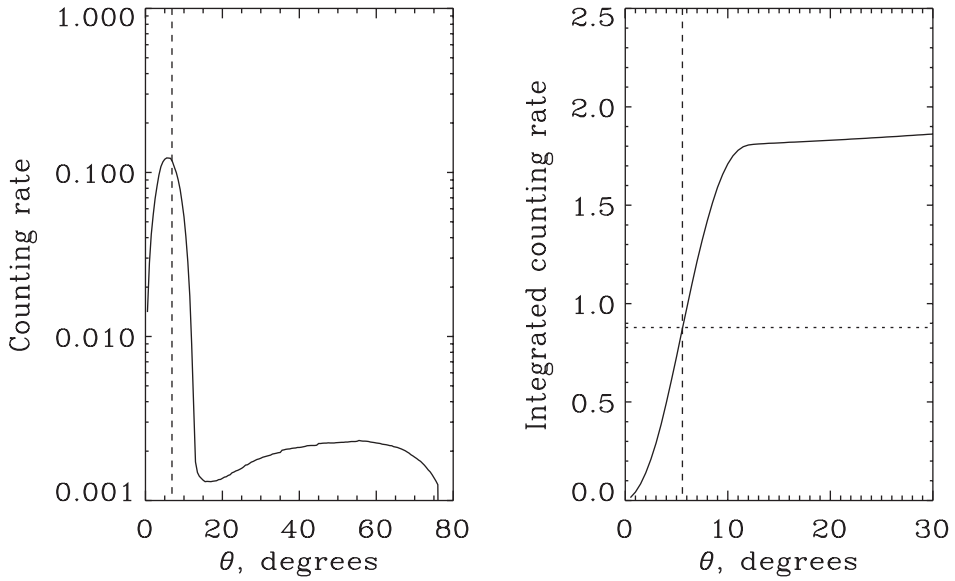

FIG. 5. Differential (left) and integral (right) plots of LEND "collimation curves," as the distribution of counts for detected neutrons from the lunar surface as a function of the angle θ from the axis of the instrument and as the number of counts for neutrons with directions within the angle , respectively (four counters CSETN 1–4 are taken together). Dashed vertical lines correspond to the angle θ_{spot} of test spot with radius of 5 km, and the dotted horizontal line corresponds to the total number of counts from the test spot.

and 2.1 counts/sec for counting rates C_{signal} and C_{tot}, respectively, one could estimate the relative amplitude of detectable variation δ_{det} about 0.03. The corresponding detectable content of hydrogen is about 80 ppm (see Fig. 4); therefore, LEND corresponds to the baseline mission requirement, as it is stated above.

However, it is well understood that actual cold traps with potential deposits of water ice are not positioned exactly at the poles but are shifted outward by several degrees of latitude. The exposure time for these spots decreases dramatically, because spatial coverage by LRO in polar orbit decreases rapidly as the spacecraft moves farther from the poles. In the next section, we present estimates for hydrogen detection limits for the polar shadowed craters, which are the main candidates for spots with water-ice deposits. They are determined by the lunar relief data presently available.

6. Expected Detection Levels of Hydrogen Enhancement in Polar Shadowed Craters

LEND will perform global mapping of the entire Moon with the same FOV of 5.6°. At moderate latitudes and at the equator the integrated exposure time for corresponding surface elements will dramatically decrease in comparison with the poles, because only a fraction of crossing orbits will contribute to observation time. However, counting statistics for particular spatial elements could be increased by increasing the surface area. Some surface features of hydrogen enhancement with large contrast may be imaged with the spatial resolution of the instrument FOV, but for most moderate latitude regions the data will be combined into pixels as large as about 20–30 km.

In reality, the major targets of LEND observations are the permanently shadowed craters distributed around the poles. We have calculated detection limits of hydrogen for some known craters, having taken into account the presently available data for landscape around them from Clementine (Rosiek and Aeschliman, 2001) and for the predicted LRO orbit; it has been demonstrated that LEND will have sufficiently high sensitivity for detection of enhanced hydrogen (or deposits of water ice) at these spots.

To perform this analysis, 2 sets of lunar craters were selected from the northern and southern polar regions of the Moon (Fig. 6). The position of southern cold traps lie above the 87°S latitude belt. Their shadowed surfaces range from 145 up to 580 km^2. The northern cold traps have centers located above the 88°N latitude belt, and their shadowed surfaces range from 148 up to 170 km^2. Table 3 shows the results of a numerical simulation of LEND detection limits for hydrogen content inside 8 of the most promising targets; there are 3 northern and 5 southern targets. It can be seen that LEND will be able to detect the presence of hydrogen ranging from 30 up to 150 ppm for the selected cold traps. The corresponding limit for detection of water ice is also presented (in weight %) for these candidate craters (Table 3). It varies from 0.03 to 0.15 wt% of water in the regolith.

7. Discussions

Testing for the presence or absence of water-ice deposits in permanently shadowed polar craters is one of the most important directions of current lunar investigations in that it will help determine the future stages of lunar exploration. LEND, along with the other instruments of the LRO payload, will have the capability to provide conclusive data with which to address the water-ice issue. The sensitivity of LEND is characterized by the hydrogen detection limit of about 100 ppm for a polar reference area with a radius of 5 km; this corresponds to the presence of about 0.1 wt% of water ice in the regolith of this spot at the pole. It may be true that re-

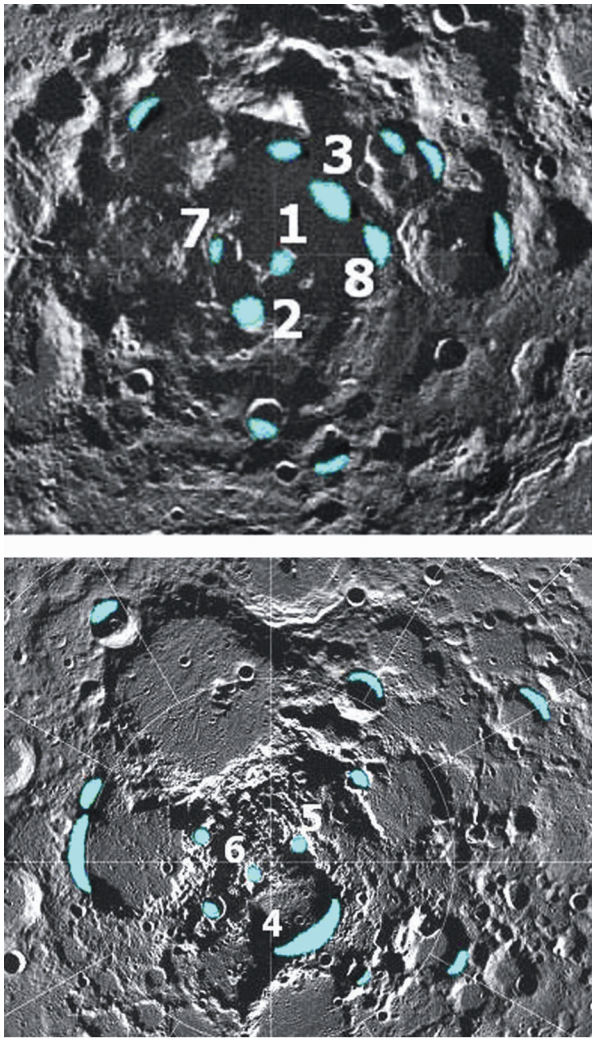

FIG. 6. Expected cold traps at the southern pole area (top) and northern pole area (bottom) of the Moon for estimation of LEND sensitivity for detection of hydrogen in the regolith. The numbered sites correspond to those in Table 3. The scale is the same on both pictures. The relief maps are based on the altitude data from Clementine (see Rosiek and Aeschliman, 2001).

gions with a much larger fraction of ice in the soil—as high as 10–30 wt% or even higher—are present. Therefore, the amount of water ice in the cold trap could actually be about 100–300 times larger than the detection limit of the reference spot with 0.1 wt% of water ice. LEND may be able to detect such a strong signature of water-ice deposits, even after the very first orbital coverage of the polar regions of the Moon, and deliver these data to the LCROSS team for better pointing of the Lunar Impactor.

On the other hand, it cannot be said that LEND is more sensitive than necessary to meet LRO objectives. A conclusive statement on the presence or absence of deposits of water ice around the poles (Task 1) could only be based on the joint analysis of data from all LRO instruments. Cold traps around poles could have enrichment of hydrogen either due to a higher concentration of implanted ions of solar wind in the regolith or due to deposits of water ice; LEND would detect in both cases the signature of a deficit of neutron emission from these regions. However, the image of the surface signature of this deficit should be quite different for these 2 cases. In the case of implantation, it would be expected that hydrogen content follow the isotherm lines, decreasing smoothly from higher to lower temperatures. On the other hand, the contour of water-ice deposits should follow the line of permanent shadow from sunlight, because outside these regions condensation of water vapor on the surface is impossible. Therefore, the maps of epithermal neutron emission should be studied together with thermal imaging data from DLRE and surface relief data from LOLA (see Chin *et al.*, 2007). DLRE and LOLA have very high spatial resolution of about 500 m and 50 m, respectively, and the horizontal scale of isotherms and shadowed regions should be a few kilometers. Therefore, LEND data with spatial resolution of 5 km (HWHM) will be appropriate for meeting the objective of Task 1. It should be noted at this point that a neutron instrument with even higher resolution, such as 3 km HWHM or so, would be technically possible, though the mass of this instrument for the same level of sensitivity would be several times larger and exceed the practical limits of total LRO science payload.

There are several discussions in the literature which suggest that neutron data from Lunar Prospector may be sufficient for resolving the issues of hydrogen / water ice at po-

TABLE 3. RESULTS OF NUMERICAL SIMULATION OF LEND DETECTION LIMIT CONCERNING SEARCH FOR HYDROGEN CONTENT INSIDE COLD TRAPS

LEND candidate targets of cold traps with possible water-ice deposits (coordinates and surface area are indicated)	*LEND hydrogen detection level limit (in ppm)*	*LEND sensitivity of water-ice deposits (in wt%)*
No. 1: (89.9°S, 111.1°E) 380 km^2	31	0.03
No. 2: (88.5°S, 220.0°E) 400 km^2	76	0.07
No. 3: (87.6°S, 38.0°E) 580 km^2	80	0.07
No. 4: (88.6°N, 32.0°E) 170 km^2	114	0.10
No. 5: (89.2°N, 122.5°E) 110 km^2	122	0.11
No. 6: (89.0°N, 291.2°E) 148 km^2	136	0.13
No. 7: (88.4°S, 260.2°E) 145 km^2	141	0.13
No. 8: (86.8°S, 75.8°E) 257 km^2	152	0.14

lar craters. These conclusions were based on results obtained by enhancing the spatial resolution of the non-collimated neutron maps from Lunar Prospector with image reconstruction methods (*e.g.,* Elphic *et al.*, 2005). In this process, estimates of the instrument FOV and statistical counting noise were used to de-blur or sharpen image features, thereby increasing the map resolution. For non-collimated neutron mapping, the 30–50 km altitude defines a large, visible lunar region of about 45–75 km (*e.g.,* see Maurice *et al.*, 2004) over which neutron counts are collected during instrument integrations. Discrimination of the exact surface point of emission of detected neutrons is not possible in this instrument configuration. Instead, with the use of orbital ephemeredes, detected counts are statistically distributed to the visible portion of the map grid, which results in image blur. Map signals are further degraded by counting noise, which is improved only by increasing map counts through repeated flyovers. Image reconstruction attempts to rectify these effects are ultimately dependent on transform implementation, which may include unjustified transform prior assumptions and a lack of justifiable convergence constraints. Also, in some transform configurations, high-frequency spurious artifacts can be induced to the map and amplified, thus yielding increased localized errors (McClanahan *et al.*, 2007). Further, these issues are exacerbated by low signal to noise and large FOV conditions.

Minimizing the instrument FOV through collimation effectively reduces the surface area of coverage and, thereby, minimizes the sampled area for a given altitude. This effectively reduces the spatial error in estimating the surface emission point (degree of blur) and facilitates detection of smaller-scale surface features. Assuming uniform spatial emissions and similar detector efficiencies, commensurate reductions in the covered area by the collimated approach also yield fewer detected counts per sample. However, the issue is offset by requiring greater surface coverage, *e.g.,* more required flyover time. Therefore, given sufficient counting statistics, to prove unambiguously the existence of surface features of several km size would require an instrument with spatial resolution that exceeds the non-collimated approach. Without such resolution, only model-dependent estimates of the scale of surface features and absolute intensities could be made.

Experience from LEND development and investigations of the Moon by this instrument may be useful for planning future missions to other celestial bodies in the Solar System that have no atmosphere or an atmosphere thin enough for orbital neutronography of the surface. Recent data from the GRS instrument suite on Mars Odyssey has shown that Mars has extremely variable neutron emission over the entire surface and huge regions with high hydrogen content around the poles and at the equatorial belt. In the case of Mars, we are reasonably sure that a high content of hydrogen means a high content of water in the soil, and that, for regions above 40–50 degrees latitude, the water is water ice (Mitrofanov *et al.*, 2007) with a mass fraction large enough to conclude that ice is one of the major constituents of the soil in these regions. We do not know the form of water in the soil at moderate latitudes below 40°; it could be chemically bound water in minerals, physically adsorbed water on the surface of regolith grains, or even water ice at some particular spots with low sunlight heating. To study water on Mars, analysis of neutron data together with data from IR and visual light would be needed, though much better neutron data resolution than the 200–300 km accomplished with Odyssey would be required.

It can be expected that some future mission will carry a neutron telescope for neutronography of Mars. At an orbital altitude of 400 km, LEND, as it is now designed, would provide neutron emission maps of the martian surface with spatial resolution (HWHM) of 40 km, about 30–60 times smaller area than we have now. Therefore, an instrument like LEND could, at some time in the future, provide global reconnaissance of the martian surface with the capability to detect regions of 40 km size on the surface of Mars with maximal content of water in the soil. These spots, provided they are selected with regard to thermal emission, relief, and geology, could become potential sites for future landers and sample return missions. We know that Mars does not have an active biosphere, though it is possible that life may have taken refuge in shallow subsurface oases. Astrobiological missions to Mars will likely target these spots at some time in the future, with data from LEND-like neutron telescopes providing navigation for them.

Abbreviations

CSETN, Collimated Sensors of EpiThermal Neutrons; DLRE, Diviner Lunar Radiometer Experiment; FOV, Field of View; GRS, Gamma-Ray Spectrometer; HEND, High Energy Neutron Detector; HWHM, Half Width Half Maximum; LAMP, Lyman-Alpha Mapping Project; LEND, Lunar Exploration Neutron Detector; LOLA, Lunar Orbiter Laser Altimeter; LRO, Lunar Reconnaissance Orbiter; MC, Module of Collimation; MSE, Module of Sensors and Electronics; SETN, Sensor of EpiThermal Neutrons; SHEN, Sensor for High Energy Neutrons; STN, Sensors of Thermal Neutrons; wt%, weight %.

References

Bobrovnitskii, Yu.I. and Korotkov, M.P. (2001) Improved estimates for the energy characteristics of a vibrating elastic structure via the input impedance and mobility: experimental verification. *Journal of Sound and Vibration* 247:683–702.

Boynton, W.V., Feldman, W.C., Squyres, S.W., Prettyman, T.H., Brückner, J., Evans, L.G., Reedy, R.C., Starr, R., Arnold, J.R., Drake, D.M., Englert, P.A.J., Metzger, A.E., Mitrofanov, I., Trombka, J.I., d'Uston, C., Wänke, H., Gasnault, O., Hamara, D.K., Janes, D.M., Marcialis, R.L., Maurice, S., Mikheeva, I., Taylor, G.J., Tokar, R., and Shinohara, C. (2002) Distribution of hydrogen in the near surface of Mars: evidence for subsurface ice deposits. *Science* 297:81–85.

Boynton, W.V., Feldman, W.C., Mitrofanov, I.G., Evans, L.G., Reedy, R.C., Squyres, S.W., Starr, R., Trombka, J.I., D'Uston, C., Arnold, J.R., Englert, P.A.J., Metzger, A.E., Wänke, H., Brückner, J., Drake, D.M., Shinohara, C., Fellows, C., Hamara, D.K., Harshman, K., Kerry, K., Turner, C., Ward, M., Barthe, H., Fuller, K.R., Storms, S.A., Thornton, G.W., Longmire, J.L., Litvak, M.L., and Ton'chev, A.K. (2004) The Mars Odyssey Gamma-Ray Spectrometer instrument suite. *Space Sci. Rev.* 110:37–83.

Chin, G., Brylow, S., Foote, M., Garvin, J., Kasper, J., Keller, J., Litvak, M., Mitrofanov, I., Paige, D., Raney, K., Robinson, M.,

Sanin, A., Smith, D., Spence, H., Spudis, P., Stern, S.A., and Zuber, M. (2007) Lunar Reconnaissance Orbiter overview: the instrument suite and mission. *Space Sci. Rev.* 129:391–419.

Crider, D.H. and Vondrak, R.R. (2000) The solar wind as a possible source of lunar polar hydrogen deposits. *J. Geophys. Res.* 105:26773–26782.

Drake, D.M., Feldman, W.C., and Jakosky, B.M. (1988) Martian neutron leakage spectra *J. Geophys. Res.* 93:6353–6368.

D'Uston, C., Atteia, J.-L., Barat, C., Chernenko, A., and Dolidze, V. (1989) Observation of the gamma-ray emission from the martian surface by the APEX experiment. *Nature* 341:598–600.

Elphic, R.C., Lawrence, D.J., Feldman, W.C., Prettyman, T.H., Maurice, S., Bussey, D.B.J., Spudis, P.D., and Lucey, P.G. (2005) Using models of permanent shadow to constrain lunar polar water ice abundances [abstract 2297]. In *36th Annual Lunar and Planetary Science Conference Abstracts,* Lunar and Planetary Institute, Houston.

Feldman, W. and Drake, D. (1986) A Doppler filter technique to measure the hydrogen content of planetary surfaces. *Nucl. Instrum. Methods Phys. Res., Sect. A* A245:182–190.

Feldman, W.C., Maurice, S., Binder, A.B., Barraclough, B.L., Elphic, R.C., and Lawrence, D.J. (1998) Fluxes of fast and epithermal neutrons from Lunar Prospector: evidence for water ice at the lunar poles. *Science* 281:1496–1500.

Feldman, W.C., Lawrence, D.J., Elphic, R.C., Barraclough, B.L., Maurice, S., Genetay, I., and Binder, A.B. (2000) Polar hydrogen deposits on the Moon. *J. Geophys. Res.* 105:4175–4196.

Feldman, W.C., Boynton, W.V., Tokar, R.L., Prettyman, T.H., Gasnault, O., Squyres, S.W., Elphic, R.C., Lawrence, D.J., Lawson, S.L., Maurice, S., McKinney, G.W., Moore, K.R., and Reedy, R.C. (2002) Global distribution of neutrons from Mars: results from Mars Odyssey. *Science* 297:75–78.

Haskin, L. and Warren, P. (1995) Lunar chemistry. In *Lunar Sourcebook,* edited by G. Heiken, D.T. Vaniman, and B.M. French, Cambridge University Press, Cambridge, pp 357–474.

Lawrence, D.J., Feldman, W.C., Elphic, R.C., Hagerty, J.J., Maurice, S., McKinney, G.W., and Prettyman, T.H. (2006) Improved modeling of Lunar Prospector neutron spectrometer data: implications for hydrogen deposits at the lunar poles. *J. Geophys. Res.* 111, E08001.

Maurice, S., Lawrence, D.J., Feldman, W.C., Elphic, R.C., and Gasnault, O. (2004) Reduction of neutron data from Lunar Prospector. *J. Geophys. Res.* 109, E07S04.

McClanahan, T.P., Trombka, J.I., Mitrofanov, I.G., and Sagdeev, R.Z. (2007) Application of image restoration (Jansson Van-Cittert) planetary remote sensing neutron count rate maps [abstract 2408]. In *38th Lunar and Planetary Science Conference Abstracts,* Lunar and Planetary Institute, Houston.

Metzger, A.E., Trombka, J.I., Peterson, L.E., Reedy, R.C., and Arnold, J.R. (1973) Lunar surface radioactivity: preliminary results of the Apollo 15 and Apollo 16 gamma-ray spectrometer experiments. *Science* 179:800–803.

Mitrofanov, I., Anfimov, D., Kozyrev, A., Litvak, M., Sanin, A., Tret'yakov, V., Krylov, A., Shvetsov, V., Boynton, W., Shinohara, C., Hamara, D., and Saunders, R.S. (2002) Maps of subsurface hydrogen from the High Energy Neutron Detector, Mars Odyssey. *Science* 297:78–81.

Mitrofanov, I.G., Zuber, M.T., Litvak, M.L., Boynton, W.V., Smith, D.E., Drake, D., Hamara, D., Kozyrev, A.S., Sanin, A.B., Shinohara, C., Saunders, R.S., and Tretyakov, V. (2003) CO_2 snow depth and subsurface water-ice abundance in the northern hemisphere of Mars. *Science* 300:2081–2084.

Mitrofanov, I.G., Zuber, M.T., Litvak, M.L., Demidov, N.E., Sanin, A.B., Boynton, W.V., Gilichinsky, D.A., Hamara, D., Kozyrev, A.S., Saunders, R.D., Smith, D.E., and Tretyakov, V.I. (2007) Water ice permafrost on Mars: layering structure and subsurface distribution according to HEND/Odyssey and MOLA/MGS data. *Geophys. Res. Lett.* 34:L18102–L18105.

Nozette, S., Lichtenberg, C.L., Spudis, P., Bonner, R., Ort, W., Malaret, E., Robinson, M., and Shoemaker, E.M. (1996) The Clementine bistatic radar experiment. *Science* 274:1495–1498.

Rosiek, M. and Aeschliman, R. (2001) Lunar shaded relief map updated with Clementine data [abstract 1943]. In *32nd Annual Lunar and Planetary Science Conference Abstracts,* Lunar and Planetary Institute, Houston.

Tomilina, T.M., Bobrovnitskii, Yu.I., Letunovsky, V.M., and Mitrofanov, I.G. (2003) Light weight vibroisolation system for high precision space instruments. In *Proceedings of the 10th International Congress of Sound and Vibration,* Stockholm, Sweden.

Vinogradov, A.P., Surkov, Yu.A., Chernov, G.M., Kirnozov, F.F., and Nazarkina, G.B. (1966) Measurements of gamma radiation of the lunar surface by the Luna-10 space station. *Cosmic Research* 4:751–755.

Address reprint requests to:
I.G. Mitrofanov
Institute for Space Research
Profsojuznaja 84/32
Moscow 117997
Russia

E-mail: mitrofanov@l503.iki.rssi.ru